Studies of the Electronic Properties of the Tetrathiotungstate(VI) Ion, $[WS_4]^{2-}$, by Low-temperature Absorption and Resonance Raman Spectroscopy

Robin J. H. Clark,* Trevor J. Dines, and Graeme P. Proud
Christopher Ingold Laboratories, University College London, 20 Gordon Street, London WC1H 0AJ

The resonance Raman spectrum of the $[WS_4]^{2-}$ ion as its $[NH_4]^+$ and $[NBu_4]^+$ salts has been studied over the range 647.1—350.7 nm. On the basis of the observed $\nu_1(a_1)$ band progressions, values for the harmonic wavenumber (ω_1) and anharmonicity constant (x_{11}) are calculated and the bandwidths are discussed in terms of contemporary theories. Computer simulation of the observed excitation profiles of the ν_1, $2\nu_1$, and $3\nu_1$ bands in the case of the $[NBu_4]^+$ salt allows the deduction that, on excitation from the ground ($^1A_1$) to resonant excited ($^1T_2$) states, the W–S bond length increases by 0.058 Å.

Recently, we reported some electronic absorption and resonance Raman (r.R.) spectroscopic studies on the tetrathiomolybdate(VI) ion, $[MoS_4]^{2-}$.[1] The r.R. spectrum of the analogous tetrathiotungstate(VI) ion, $[WS_4]^{2-}$, has not yet been reported presumably because the longest wavelength absorption band, $\lambda_{max.} \simeq 395$ nm ($\varepsilon_{max.} = 15\,000$ dm^3 mol^{-1} cm^{-1}) for the species in solution,[2,3] is outside the range of the commonly available laser excitation lines. This band is assigned to the lowest energy ligand-to-metal charge-transfer transition $^1T_2 \leftarrow {}^1A_1$ ($e^1t_1{}^5 \leftarrow t_1{}^6$) and is the analogue of the band at 470 nm in the spectrum of $[MoS_4]^{2-}$.

The availability of Kr^{2+} laser and dye laser excitation in the 400 nm region has enabled us to obtain r.R. spectra of both the $[NH_4]^+$ and $[NBu_4]^+$ salts of $[WS_4]^{2-}$ in the solid state at low temperature. Additionally, we have measured electronic absorption spectra of the ion at low temperature in order to achieve better resolution than that obtained in the room-temperature solution spectra previously reported and, together with the r.R. data, this enables a more detailed analysis of the lowest energy $^1T_2$ excited state to be made.

Experimental

The sample of $[NH_4]_2[WS_4]$ used in this study was supplied by Dr. J. R. Dilworth, University of Sussex. $[NBu_4]_2[WS_4]$ was prepared metathetically from $[NBu_4]Br$ and $[NH_4]_2[WS_4]$, and was recrystallized from propan-2-ol. Resonance Raman spectra were obtained from KBr and KBr–$K[NO_3]$ discs at *ca.* 80 K using a liquid-nitrogen cooled cell. To minimize thermal decomposition a cylindrical lens was employed to obtain a line focus of the laser excitation beam on the sample and the laser power was maintained at <50—60 mW.

Raman spectra were recorded on Spex 1401 and 14018 (Ramalog 6) spectrometers in conjunction with Coherent Radiation model CR15 u.v. argon ion and CR3000K krypton ion lasers and a CR599 dye laser employing stilbene 1 as the lasing medium (tuning range 397—426 nm). Detection of the scattered radiation was by standard photon-counting techniques, using RCA C31034 photomultipliers. Wavenumber measurements were calibrated with the emission spectrum of neon, and band intensities were determined as the products of peak heights and full-width half-maxima (f.w.h.m.) and corrected for the spectral response of the instrument. The r.R. excitation profiles were constructed using the 1 050 cm^{-1} band of $K[NO_3]$ as internal standard.

Electronic spectra were recorded on a Cary 14 spectrometer from KBr discs at *ca.* 14 K using an Air Products Displex cryostat in association with a Leybold-Heraeus turbopump type TM120.

Table 1. Details of the r.R. spectrum of $[WS_4]^{2-}$ at 80 K ($\lambda_0 = 406.7$ nm)

Assignment	$\tilde{\nu}$/cm^{-1}	f.w.h.m./ cm^{-1}	Relative intensity
(*a*) $[NH_4]_2[WS_4]$			
$\nu_2(e)$	173 ± 2		<0.01
$\nu_4(t_2)$	187 ± 2		<0.01
$\nu_3(t_2)$ [a]	461.0 ± 1.0		0.15
$\nu_1(a_1)$ [b]	488.0 ± 0.5	8.6 ± 0.5	1.00
$\nu_1 + \nu_3(T_2)$	945 ± 2		
$2\nu_1(A_1)$ [b]	975.2 ± 1.0	15.8 ± 1.0	0.36
$3\nu_1(A_1)$ [b]	1 459 ± 1	21 ± 1	0.23
$4\nu_1(A_1)$	1 941 ± 2	27 ± 1	0.12
$5\nu_1(A_1)$	2 426 ± 2	33 ± 2	0.06
$6\nu_1(A_1)$	2 895 ± 5	37 ± 2	0.03
(*b*) $[NBu_4]_2[WS_4]$			
$\nu_3(t_2)$	463.3 ± 1.0 [c]		
$\nu_1(a_1)$	477.6 ± 0.5	6.2 ± 0.5	1.00
$2\nu_1(A_1)$	955.0 ± 1.0	8.2 ± 1.0	0.32
$3\nu_1(A_1)$	1 433 ± 1	12 ± 1	0.16
$4\nu_1(A_1)$	1 905 ± 1	19 ± 1	0.07
$5\nu_1(A_1)$	2 379 ± 2		0.03

[a] At 462 cm^{-1}, by i.r. spectroscopy. [b] Depolarisation ratio $\rho < 0.01$ in aqueous NH_3 solution with 406.7 nm excitation. [c] At 463 cm^{-1} by i.r. spectroscopy.

Results

The r.R. spectrum of $[WS_4]^{2-}$ is dominated by an overtone progression $v_1\nu_1$ extending to $v_1 = 7$ for the $[NH_4]^+$ salt and to $v_1 = 5$ for the $[NBu_4]^+$ salt. There is also a very weak progression in ν_1 based on single quanta of one or both of the deformation modes $\nu_2(e)$ and $\nu_4(t_2)$, and a progression $v_1\nu_1 + \nu_3$ which is overlapped by the $v_1\nu_1$ progression. The spectra obtained with 406.7 nm excitation are shown in Figures 1 and 2 and wavenumber measurements, bandwidths, and relative intensities are given in Table 1.

Raman spectra of both salts were recorded for excitation in the range 350.7—647.1 nm. Excitation profiles were constructed for those Raman bands which were sufficiently intense to provide reliable data. The excitation profiles are shown in Figures 3 and 4 together with the absorption spectra recorded at 14 K. In the case of the $[NBu_4]^+$ salt partial resolution of vibronic structure is observed in the absorption spectrum, from which it is determined that the 0–0 transition

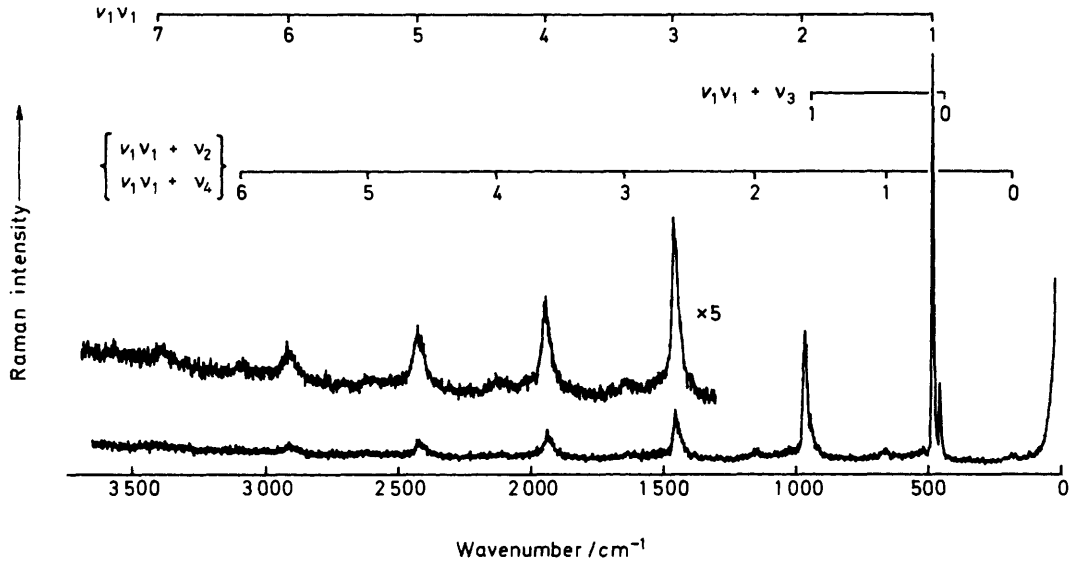

Figure 1. Resonance Raman spectrum of $[NH_4]_2[WS_4]$ at 80 K recorded with 406.7 nm excitation. Power at the sample = 50 mW, spectral slit width = 4 cm^{-1} at 406.7 nm, scanning speed = 1 cm^{-1} s^{-1}, and time constant = 1 s

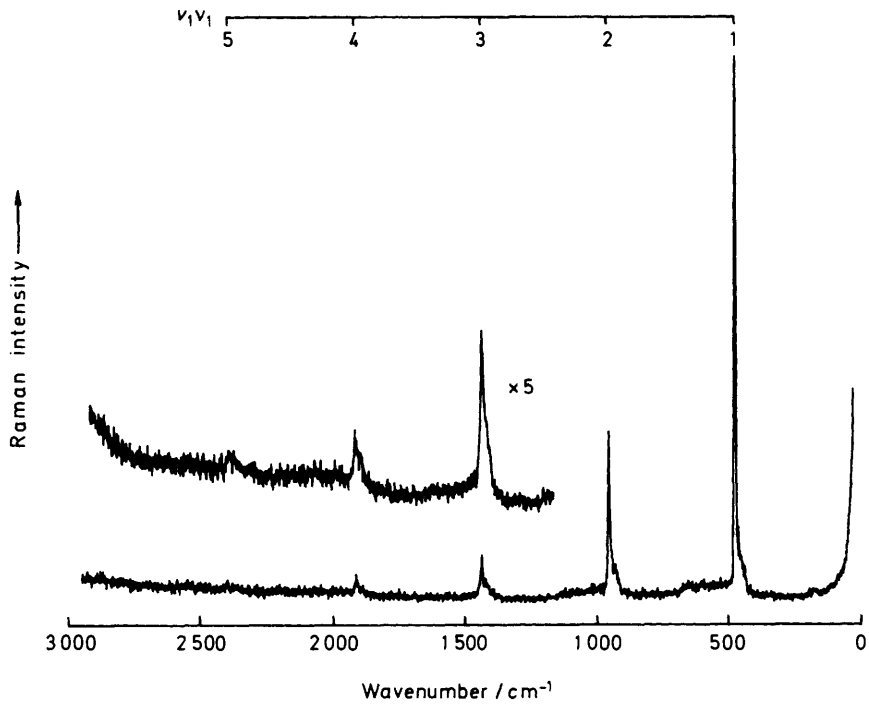

Figure 2. Resonance Raman spectrum of $[NBu_4]_2[WS_4]$ at 80 K recorded with 406.7 nm excitation. Experimental details as for Figure 1

wavenumber is 24 510 ± 20 cm^{-1} and the vibrational spacing is 410 ± 20 cm^{-1}.

Discussion

Vibrational Analysis.—The measurements of the wavenumbers of the v_1v_1 progressions for the two salts permit the determination of the anharmonicity constant x_{11} and an approximate value for the harmonic wavenumber ω_1. For $[NH_4]_2[WS_4]$ it was calculated that $\omega_1 = 490.5 \pm 0.5$ cm^{-1} and $x_{11} = -1.1 \pm 0.1$ cm^{-1}, and for $[NBu_4]_2[WS_4]$ that $\omega_1 = 478.4 \pm 0.5$ cm^{-1} and $x_{11} = -0.44 \pm 0.05$ cm^{-1}. The significantly lower value of ω_1 for the $[NBu_4]^+$ salt may be rationalised in terms of its larger lattice dimensions relative to those of the $[NH_4]^+$ salt. Thus the variation in ω_1 with the nature of the counter ion for the $[MnO_4]^-$ ion in a variety of different host lattices [4] is such that the lowest ω_1 values occur for salts involving the most space-filling cations ($[NBu_4]^+$ and $[PPh_4]^+$). The different x_{11} values obtained for the two salts probably also result from the different lattice dimensions, but in both cases the v_1 mode of the $[WS_4]^{2-}$ ion very nearly behaves as a harmonic oscillator. This is found to be the case for the v_1 mode of most tetrahedral molecules and ions [5]

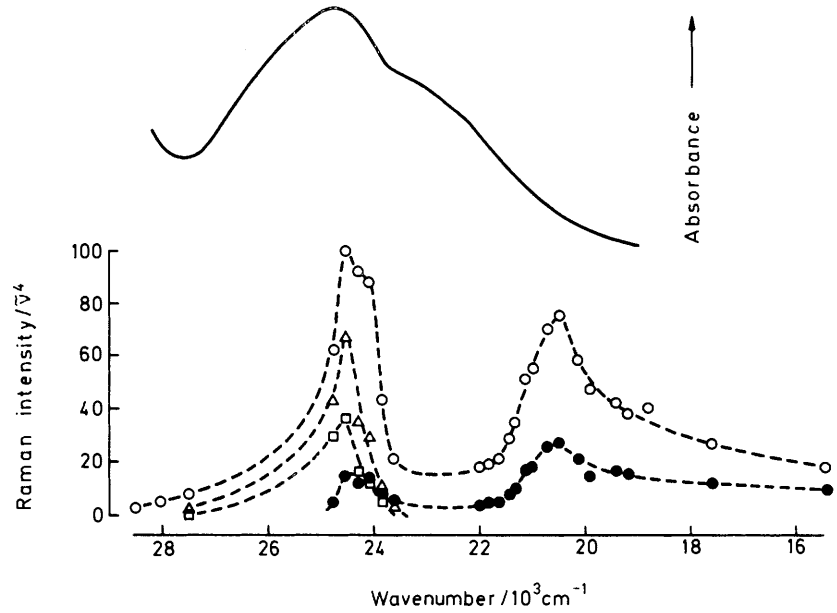

Figure 3. Electronic absorption spectrum of $[NH_4]_2[WS_4]$ at 14 K (solid line) and the excitation profiles for ν_1 (○), $2\nu_1$ (△), $3\nu_1$ (□), and ν_1 (●) at 80 K

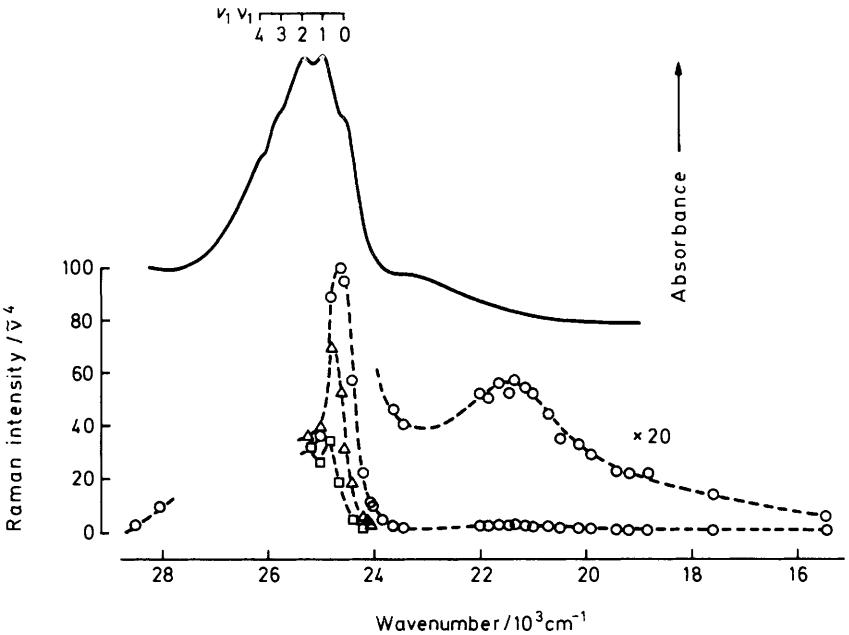

Figure 4. Electronic absorption spectrum of $[NBu_4]_2[WS_4]$ at 14 K (solid line) and the excitation profiles for ν_1 (○), $2\nu_1$ (△), and $3\nu_1$ (□) at 80 K

Bandwidths.—It is well established that, for r.R. overtone progressions of the type $v_i\nu_i$, the bandwidths of the members increase with increasing v_i. A theory of r.R. bandwidths for species in liquids and solutions has been developed by Madden and co-workers,[6-8] in which it is shown that the variation of f.w.h.m. with v_i may be either linear or quadratic. The latter behaviour is observed when the time-scale for vibrational relaxation and dephasing processes is long compared to that for molecular motion (' fast modulation limit '). Slow modulation, by contrast, results in a linear dependence of f.w.h.m. on v_i. Although it is not clear whether Madden's theory is strictly valid for solid species, we have plotted the f.w.h.m.'s of the members of the $v_1\nu_1$ progressions observed for $[NH_4]_2[WS_4]$ and $[NBu_4]_2[WS_4]$ against v_1 and v_1^2. The results, shown in Figure 5, indicate that v_1 dependence is exhibited by $[NH_4]_2[WS_4]$ and v_1^2 dependence by $[NBu_4]_2[WS_4]$. This difference in behaviour for the two salts may be related either to the larger number of degrees of freedom for $[NBu_4]^+$ ($3N - 6 = 153$) than for $[NH_4]^+$ ($3N - 6 = 9$), or to the different lattice dimensions.

Electronic Absorption Spectra and Excitation Profiles.—The electronic spectrum of $[WS_4]^{2-}$ in the 400—450 nm region consists of a band at *ca.* 400 nm and a shoulder at longer

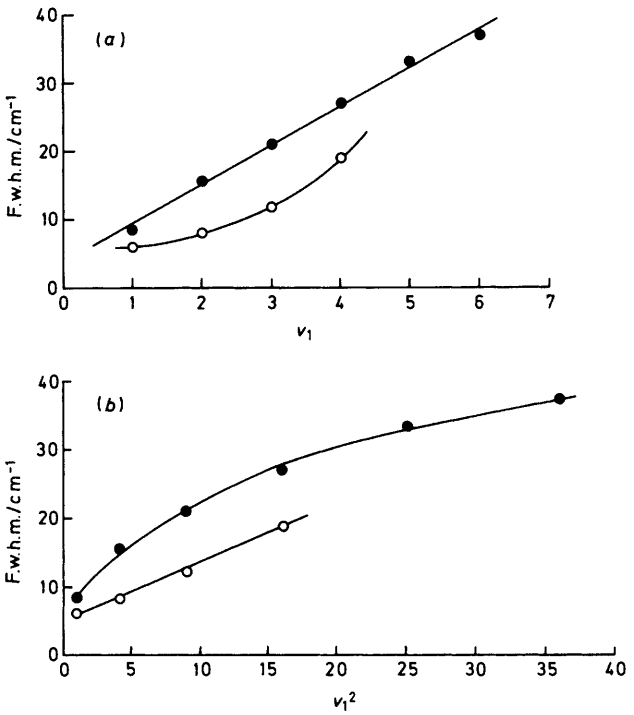

Figure 5. Plots of f.w.h.m. (cm^{-1}) *versus* (*a*) v_1 and (*b*) v_1^2 for the members of the v_1v_1 progressions of $[NH_4]_2[WS_4]$ (●) and $[NBu_4]_2[WS_4]$ (○)

wavelength. The 400 nm band has been assigned to the $^1T_2 \leftarrow {}^1A_1$ transition resulting from the excitation of an electron from the t_1 non-bonding orbital, localized on the ligands, to the e metal–ligand antibonding orbital.[2,3] Such an excitation can give rise to three other transitions, namely $^1T_1 \leftarrow {}^1A_1$, $^3T_2 \leftarrow {}^1A_1$, and $^3T_1 \leftarrow {}^1A_1$, and the shoulder observed at *ca.* 430 nm must be due to one of these as there can be no other electronic transitions of lower energy. Of these three transitions one is orbitally forbidden ($^1T_1 \leftarrow {}^1A_1$), one is spin forbidden ($^3T_2 \leftarrow {}^1A_1$) and the third is both spin and orbitally forbidden ($^3T_1 \leftarrow {}^1A_1$). Since the last would violate both spin and orbital selection rules it may be ruled out on intensity grounds as a credible assignment for the 430 nm shoulder. The $^1T_1 \leftarrow {}^1A_1$ transition could acquire intensity as a result of either (*a*) lowering in symmetry of the $[WS_4]^{2-}$ ion in the solid state or (*b*) vibronic mixing of the $^1T_2$ and $^1T_1$ states *via* either or both of the e and t_2 class vibrations. On the other hand a spin–orbit interaction of significant magnitude might cause the $^3T_2$ excited state to be mixed with singlet excited states, with the result that the $^3T_2 \leftarrow {}^1A_1$ transition would become allowed. However, such an effect cannot be important since the assignment of the 430 nm shoulder must be consistent with the observation that it is much more intense for the $[NH_4]^+$ salt than for the $[NBu_4]^+$ salt. Any differences in the spectroscopic properties of $[WS_4]^{2-}$ in these two salts must therefore be related to their different lattice dimensions. $[NH_4]_2[WS_4]$ has a more tightly packed lattice than $[NBu_4]_2[WS_4]$, as evidenced by the higher $\nu_1(a_1)$ band wavenumber, and this causes a larger perturbation of the $[WS_4]^{2-}$ electronic energy levels. For this reason, we favour the $^1T_1 \leftarrow {}^1A_1$ assignment for the 430 nm shoulder and corroborative evidence is provided by the observation of, and analogous assignment for, similar bands in the spectra of salts of the $[CrO_4]^{2-}$ and $[MnO_4]^-$ ions.[9–13] Moreover, for the ammonium salt the 430 nm shoulder is much weaker relative to the main $^1T_2 \leftarrow {}^1A_1$ band in aqueous ammonia than it is in the solid state, again suggesting that the intensity of the shoulder is significantly influenced by lattice effects.

The r.R. band excitation profiles of ν_1, $2\nu_1$, and $3\nu_1$ for both salts display maxima within the contour of the $^1T_2 \leftarrow {}^1A_1$ absorption band. Intensity enhancement of the ν_1 band is also observed in the vicinity of the $^1T_1 \leftarrow {}^1A_1$ band but the maximum is red-shifted from there by *ca.* 2 000 cm^{-1}. A red shift in an excitation profile maximum in the region of a weak absorption band is common for systems in which there is an intense nearby absorption band (see, for example, ref. 14) and is attributed to interference between the contributions to the scattered intensity from the two transitions (see below). The larger enhancement of $\nu_1(a_1)$ in the region of the $^1T_1 \leftarrow {}^1A_1$ transition for the $[NH_4]^+$ salt than for the $[NBu_4]^+$ salt is consistent with the larger intensity for this electronic transition (relative to that of the $^1T_2 \leftarrow {}^1A_1$ transition) in the former case.

By contrast, the intensity of the $\nu_3(t_2)$ band is greatest for excitation resonant with the $^1T_1$ state, an observation which is not yet clearly understood. Non-totally symmetric Raman bands may be subject to resonance enhancement if the relevant vibrational modes are (*a*) Jahn–Teller active in the resonant excited state (degenerate states only) or (*b*) Herzberg–Teller active, *i.e.* they vibronically couple a pair of excited electronic states. The $\nu_3(t_2)$ vibration is Jahn–Teller active in both the $^1T_1$ and $^1T_2$ states and is also able to couple these two states vibronically. Thus, the experimental observations might be interpreted in terms of the activity of ν_3 in either an inter- or an intra-manifold vibronic coupling scheme, or both.

Calculations of the ν_1 *Band Excitation Profiles.*—Using an established theoretical model for *A*-term r.R. scattering [5,15] it is possible to perform a computer simulation of r.R. excitation profiles and, in so doing, obtain valuable information pertaining to the resonant excited state. Where only a single electronic transition contributes significantly, the transition polarizability for the totally symmetric mode of a tetrahedral molecule is given by equation (1) where $|g\rangle$ is the ground

$$[\alpha_{\rho\rho}]_{gn,g0} = \frac{1}{\hbar c}|[\mu_\rho]^0_{ge}|^2 \sum_v \frac{\langle n_g|v_e\rangle\langle v_e|0_g\rangle}{\tilde{\nu}_{ev,g0} - \tilde{\nu}_0 + i\Gamma_{ev}} \qquad (1)$$

electronic state, $|e\rangle$ is the resonant excited state, and n and v are vibrational quantum numbers; Γ_{ev} represents the homogeneous linewidth, which is inversely proportional to the lifetime of the vth level of the resonant excited state. The assumptions inherent in equation (1) are that (*a*) the Born–Oppenheimer approximation is valid, (*b*) the dependence of the transition dipole moment on nuclear co-ordinates may be neglected (Condon approximation), (*c*) all molecules are initially in the zeroth vibrational level of the ground electronic state (low temperature limit), and (*d*) inhomogeneous (site) broadening is negligible. For most systems the neglect of inhomogeneous broadening is not justifiable, in that such a procedure necessitates the use of unacceptably large values of Γ_{ev} to produce a satisfactory fit to the experimental data.

Variation of the electronic transition wavenumber, $\tilde{\nu}_{eg}$, induced by the molecular environment may be described by a Lorentzian distribution (2) where $\langle\tilde{\nu}_{eg}\rangle$ is the average value

$$\mathscr{L}(\tilde{\nu}_{eg}) = \frac{\gamma}{[(\tilde{\nu}_{eg} - \langle\tilde{\nu}_{eg}\rangle)^2 + \gamma^2]} \qquad (2)$$

of the transition wavenumber and γ is the half-width associated with the inhomogeneous broadening mechanism. The transition polarizability is then given by equation (3). Siebrand and

Table 2. Parameters used in the calculations of the excitation profiles of $[NBu_4]_2[MS_4]$ in the region of the $^1T_2 \leftarrow {}^1A_1$ band

Parameter	Value: M = Mo[1]	Value: M = W	Source
$\tilde{\nu}_1^g$/cm^{-1}	451	477	Raman spectrum
$\tilde{\nu}_1^e$/cm^{-1}	410	410	Absorption spectrum
$\tilde{\nu}_{eg}$/cm^{-1}	20 230	24 650 ± 10	Best fit [a]
Δr/Å	0.07	0.058 ± 0.002	Best fit
Γ/cm^{-1}	265 [b]	100 ± 10	Best fit
γ/cm^{-1}		150 ± 20	Best fit

[a] The lower wavenumber for the 0_g–0_e transition measured from the absorption spectrum (24 510 cm^{-1}) is believed to be due to the poor resolution of the vibronic structure. The 0_g–1_e, 0_g–2_e, 0_g–3_e, and 0_g–4_e transitions occur at 24 940, 25 320, 25 710, and 26 140 cm^{-1} respectively. [b] No improvement in the quality of the best fit for $[MoS_4]^{2-}$ could be obtained by variation of Γ and γ. Nevertheless, the true value of Γ may be less than 265 cm^{-1}.

$$[\alpha_{\rho\rho}]_{gn,g0} = \frac{1}{\hbar c}|[\mu_\rho]^0_{ge}|^2 \int_\infty \left[\sum_v \frac{\langle n_g|v_e\rangle\langle v_e|0_g\rangle}{\tilde{\nu}_{ev,g0} - \tilde{\nu}_0 + i\Gamma_{ev}}\right] \mathcal{L}(\tilde{\nu}_{eg})d\tilde{\nu}_{eg} \quad (3)$$

$$I_{gn,g0}(\tfrac{\pi}{2}) = K(\tilde{\nu}_0 - \tilde{\nu}_{gn,g0})^4|[\mu_\rho]^0_{ge}|^4 \sum_v \sum_{v'} \langle n_g|v_e\rangle\langle v_e|0_g\rangle\langle n_g|v_{e'}\rangle\langle v_{e'}|0_g\rangle \left\{\frac{[(\varepsilon_v - \varepsilon_{v'})^2 + 4\Gamma\Sigma][\varepsilon_v\varepsilon_{v'} + \Sigma^2] - 2(\varepsilon_v - \varepsilon_{v'})\gamma\Sigma}{[\varepsilon_v^2 + \Sigma^2][\varepsilon_{v'}^2 + \Sigma^2][(\varepsilon_v - \varepsilon_{v'})^2 + 4\Gamma^2]}\right\} \quad (4)$$

$$I_{gn,g0}(\tfrac{\pi}{2}) = K(\tilde{\nu}_0 - \tilde{\nu}_{gn,g0})^4 \sum_{i=1}^{N}\sum_{i'=1}^{N} |[\mu_\rho]^0_{ge_i}|^2|[\mu_\rho]^0_{ge_{i'}}|^2 \sum_v \sum_{v'} \langle n_g|v_{e_i}\rangle\langle v_{e_i}|0_g\rangle\langle n_g|v_{e_{i'}}\rangle\langle v_{e_{i'}}|0_g\rangle$$
$$\left\{\frac{[(\varepsilon_v{}^i - \varepsilon_{v'}{}^{i'})^2 + (\Gamma_i + \Gamma_{i'})(\Sigma_i + \Sigma_{i'})][\varepsilon_v{}^i\varepsilon_{v'}{}^{i'} + \Sigma_i\Sigma_{i'}] - \frac{1}{2}(\varepsilon_v{}^i - \varepsilon_{v'}{}^{i'})(\gamma_i + \gamma_{i'})(\Sigma_i + \Sigma_{i'})}{[\varepsilon_v{}^{i2} + \Sigma_i^2][\varepsilon_{v'}{}^{i'2} + \Sigma_{i'}^2][(\varepsilon_v{}^i - \varepsilon_v{}^{i'})^2 + (\Gamma_i + \Gamma_{i'})^2]}\right\} \quad (5)$$

co-workers [16,17] have evaluated such integrals, and excitation profiles may be determined from equation (4) where $\varepsilon_v = \tilde{\nu}_{ev,g0} - \tilde{\nu}_0$, $\Sigma = \Gamma + \gamma$, and a common homogeneous linewidth, Γ, has been taken for all of the excited-state vibrational levels. The vibrational overlap integrals, which may be calculated using Manneback's recursion formulae,[18] are dependent on the ground- and excited-state vibrational wavenumbers for the ν_1 mode ($\tilde{\nu}_1^g$ and $\tilde{\nu}_1^e$) and the displacement, δ, of the excited-state potential energy minimum with respect to that of the ground state along the normal coordinate Q_1. The latter is related to the bond length extension, Δr, attendant upon excitation to the resonant state. Thus, the computer simulation of the experimental data, using equation (4), enables Δr to be determined. Such calculations have recently been reported for the tetrahedral ions $[MnO_4]^-$ [15] and $[MoS_4]^{2-}$,[1] and for the radical anions S_2^- and Se_2^- trapped in ultramarine host lattices.[19]

Best-fit computer simulations of the excitation profiles of ν_1, $2\nu_1$, and $3\nu_1$ have been calculated for $[NBu_4]_2[WS_4]$ in the region of the $^1T_2 \leftarrow {}^1A_1$ absorption band, using the parameters listed in Table 2. The experimental and calculated data are shown in Figure 6 and a calculation of the overtone intensity distribution for 406.7 nm excitation is listed in Table 3, together with the experimental data. Detailed calculations were not performed on the Raman intensity data for $[NH_4]_2[WS_4]$ because the data for this salt were believed to be less reliable, but the effect of the $[NH_4]^+$ cation is to increase the inhomogeneous linewidth γ to about 600 cm^{-1} and to reduce the 0_e–0_g transition wavenumber, $\tilde{\nu}_{eg}$, by *ca.* 250—300 cm^{-1}.

Computer simulation of the ν_1 band excitation profile of the $[NBu_4]^+$ salt in the region of the $^1T_1 \leftarrow {}^1A_1$ absorption band requires a minor modification to the above theoretical model. Because the $^1T_1$ state is only 4 000 cm^{-1} below the $^1T_2$ state, the contributions from both need to be included in the transition polarizability. The excitation profile is then given by equation (5) where $\varepsilon_v{}^i = (\tilde{\nu}_{e_ig} - \tilde{\nu}_0)$ and the first two summations are over the N excited states included in the transition polarizability; $N = 2$ in the present example but in principle any number of states may be included. A best-fit computer simulation of the ν_1 band excitation profile has been calculated for $[NBu_4]_2[WS_4]$ in the region of the $^1T_1 \leftarrow {}^1A_1$ absorption band, using the parameters listed in Table 4, and the experimental and calculated data are shown in Figure 7. The values of Δr and the vibrational wavenumber of ν_1 in the $^1T_1$ state were assumed to be the same as those of the $^1T_2$ state because these states arise from the same excited configuration ($e^1t_2^5$) of $[WS_4]^{2-}$. Two features of the calculation are particularly significant: (*a*) the inhomogeneous linewidth γ is much larger for the $^1T_1$ state, and (*b*) the relative absorption intensity $|[\mu_\rho]^0_{ge_1}|^2/|[\mu_\rho]^0_{ge_2}|^2$ is calculated to be much higher than is found in the absorption spectrum (*ca.* 0.1). The first of these observations is not entirely surprising because the broadening due to the influence of the molecular environment need not be the same for every electronic transition. Indeed, the lifetimes of different excited states are not expected to be identical; in the present case a departure of more than 20 cm^{-1} from the Γ value of 100 cm^{-1} for the $^1T_1 \leftarrow {}^1A_1$ transition significantly impaired the quality of the fit. The second observation, *i.e.* that a greater absorption intensity for the $^1T_1 \leftarrow {}^1A_1$ transition is obtained from the best fit than is measured from the absorption spectrum, is much more surprising. This may be due to a *B*-term contribution to the Raman intensity, which can only occur if the site symmetry of $[WS_4]^{2-}$ is lower than T_d ($T_1 \times T_2$ does not contain the A_1 representation). It has been shown that, if $[\mu_\rho]^0_{ge_1}$ and $[\mu_\rho]^0_{ge_2}$ are polarized along the same direction, constructive interference may occur between the *A*- and *B*-term contributions in the 0_g–0_{e_1} region leading to an enhanced Raman intensity.[20] Inclusion of the $^1T_1$ excited state in the transition polarizability has a negligible (<5%) effect on the calculated excitation profiles in the region of the $^1T_2 \leftarrow {}^1A_1$ transition.

Table 3. Comparison of the experimental and calculated overtone distribution for $[NBu_4]_2[WS_4]$ (λ_0 = 406.7 nm)

ν_1	$I_{exp.}$	$I_{calc.}$
1	1.00	1.00
2	0.32	0.42
3	0.16	0.17
4	0.07	0.06
5	0.03	0.02

Conclusions

On excitation to the lowest $^1T_2$ state of the $[WS_4]^{2-}$, $[MoS_4]^{2-}$ and $[MnO_4]^-$ ions, the changes in W–S, Mo–S,[1] and Mn–O [15]

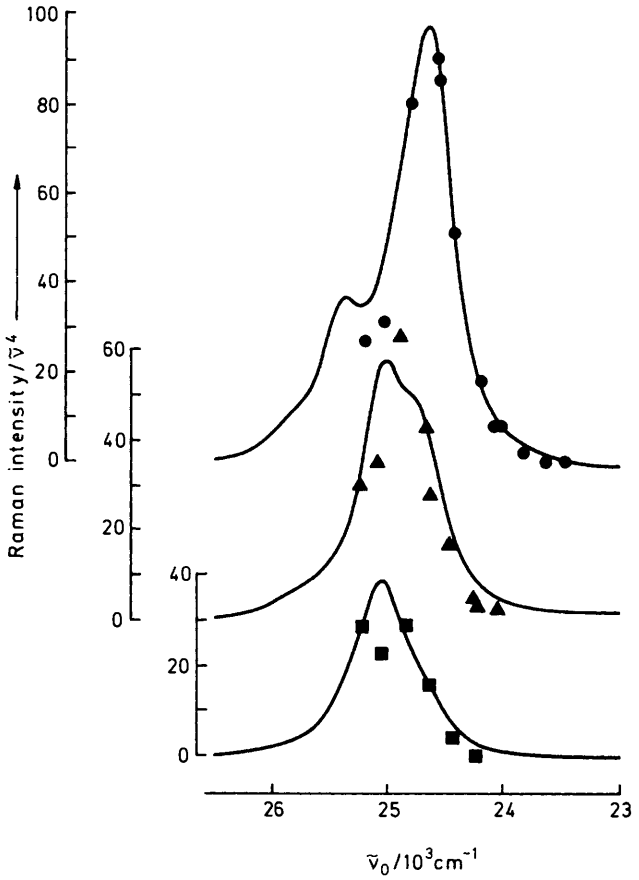

Figure 6. Calculated (solid lines) and experimental excitation profiles for the ν_1 (●), $2\nu_1$ (▲), and $3\nu_1$ (■) bands of $[NBu_4]_2[WS_4]$ at 80 K in the region of the $^1T_2 \leftarrow {}^1A_1$ absorption band

Table 4. Parameters used in the calculation of the $[NBu_4]_2[WS_4]$ ν_1 band excitation profile in the region of the $^1T_1 \leftarrow A_1$ band

Parameter *	Value	Source
$\lvert[\mu_\rho]^0_{ge_1}\rvert^2/\lvert[\mu_\rho]^0_{ge_2}\rvert^2$	0.32	Best fit
ν_{e_1g}/cm^{-1}	21 200	Best fit
Γ_1/cm^{-1}	100 ± 10	Best fit
γ_1/cm^{-1}	1 250 ± 50	Best fit

* The parameters relating to the $^1T_2 \leftarrow {}^1A_1$ transition are as listed in Table 2 and the bond length change Δr and the excited-state vibrational wavenumber associated with the $^1T_1$ state are assumed to be identical to those of the $^1T_2$ state; e_1 refers to the $^1T_1$ excited state and e_2 to the $^1T_2$ one.

bond lengths are found to be 0.058, 0.07, and 0.09 Å, respectively. It would seem therefore that the geometric changes resulting from such electronic excitation become less as the atomic number of the central metal atom increases, although many further studies of analogous transition metal tetroxo- and tetrathio-anions will be necessary in order to establish firmly this trend.

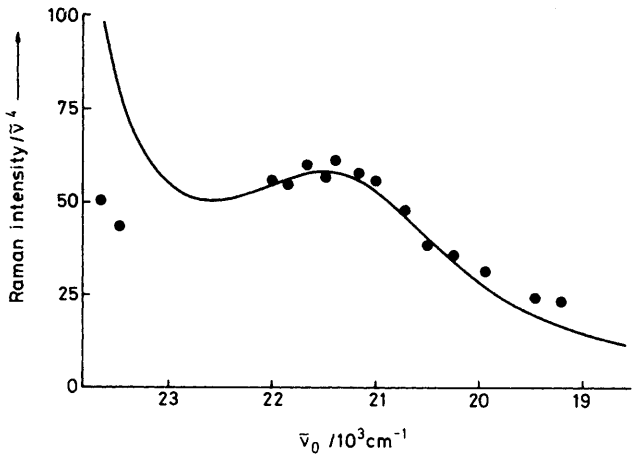

Figure 7. Calculated (solid line) and experimental (●) excitation profile for the ν_1 band of $[NBu_4]_2[WS_4]$ at 80 K in the region of the $^1T_1 \leftarrow {}^1A_1$ absorption band

Acknowledgements

We are indebted to Dr. J. R. Dilworth (University of Sussex) for the generous gift of a sample of $[NH_4]_2[WS_4]$. We thank the S.E.R.C. and the University of London (ULIRS) for financial support.

References

1 R. J. H. Clark, T. J. Dines, and M. L. Wolf, *J. Chem. Soc., Faraday Trans. 2*, 1982, 679.
2 A. Müller, E. Diemann, and C. K. Jørgensen, *Struct. Bonding (Berlin)*, 1973, **14**, 23.
3 R. H. Petit, B. Briat, A. Müller, and E. Diemann, *Mol. Phys.*, 1974, **27**, 1373.
4 R. J. H. Clark and T. J. Dines, *J. Chem. Soc., Faraday Trans. 2*, 1982, 723.
5 R. J. H. Clark and B. Stewart, *Struct. Bonding*, 1979, **36**, 1.
6 P. A. Madden and H. Wennerstrom, *Mol. Phys.*, 1976, **31**, 1103.
7 P. A. Madden and R. M. Lynden-Bell, *Chem. Phys. Lett.*, 1976, **38**, 163.
8 M. R. Battaglia and P. A. Madden, *Mol. Phys.*, 1978, **36**, 1601.
9 B. Butowiez, *C. R. Acad. Sci. Ser. B*, 1968, **267**, 1234.
10 L. W. Johnson and S. P. McGlynn, *Chem. Phys. Lett.*, 1970, **7**, 618.
11 C. J. Ballhausen and I. B. Trabjerg, *Mol. Phys.*, 1972, **24**, 689.
12 S. C. Jain, D. Pooley, and R. Singh, *J. Phys. C*, 1972, **23**, L307.
13 J. C. Collingwood, P. Day, R. G. Denning, and D. J. Robbins, *Chem. Phys. Lett.*, 1972, **13**, 567.
14 P. Stein, V. Miskowski, W. H. Woodruff, J. P. Griffin, K. G. Werner, B. P. Gaber, and T. G. Spiro, *J. Chem. Phys.*, 1976, **64**, 2159.
15 R. J. H. Clark and B. Stewart, *J. Am. Chem. Soc.*, 1981, **103**, 6593.
16 A. P. Penner and W. Siebrand, *Chem. Phys. Lett.*, 1976, **39**, 11.
17 W. Siebrand and M. Z. Zgierski, *J. Phys. Chem.*, 1982, **86**, 4718.
18 C. Manneback, *Physica*, 1951, **17**, 1001.
19 R. J. H. Clark, T. J. Dines, and M. Kurmoo, *Inorg. Chem.*, in the press.
20 R. J. H. Clark and T. J. Dines, *Chem. Phys. Lett.*, 1981, **79**, 321.

Received 2nd *February* 1983; *Paper* 3/151